

Incorporation of Antimicrobial Peptides into Membranes: A Combined Liquid-State NMR and Molecular Dynamics Study of Alamethicin in DMPC/DHPC Bicelles

Jens Dittmer,^{†,‡} Lea Thøgersen,^{†,§} Jarl Underhaug,[†] Kresten Bertelsen,[†] Thomas Vosegaard,[†] Jan M. Pedersen,[†] Birgit Schiøtt,[†] Emad Tajkhorshid,^{||} Troels Skrydstrup,[†] and Niels Chr. Nielsen^{*,†}

Center for Insoluble Protein Structures (inSPIN), Interdisciplinary Nanoscience Center (iNANO) and Department of Chemistry, University of Aarhus, Denmark, Laboratoire de Physique de l'Etat Condensé (LPEC), Université du Maine, Le Mans, France, Bioinformatics Research Center (BiRC), University of Aarhus, Denmark, and Department of Biochemistry, Beckman Institute, and Center for Biophysics and Computational Biology, University of Illinois at Urbana-Champaign, Urbana, Illinois 61801

Received: December 30, 2008; Revised Manuscript Received: February 20, 2009

Detailed insight into the interplay between antimicrobial peptides and biological membranes is fundamental to our understanding of the mechanism of bacterial ion channels and the action of these in biological host-defense systems. To explore this interplay, we have studied the incorporation, membrane-bound structure, and conformation of the antimicrobial peptide alamethicin in lipid bilayers using a combination of ¹H liquid-state NMR spectroscopy and molecular dynamics (MD) simulations. On the basis of experimental NMR data, we evaluate simple in-plane and transmembrane incorporation models as well as pore formation for alamethicin in DMPC/DHPC (1,2-dimyristoyl-sn-glycero-3-phosphatidylcholine/1,2-dihexanoyl-sn-glycero-3-phosphatidylcholine) bicelles. Peptide–lipid nuclear Overhauser effect (NOE) and paramagnetic relaxation enhancement (PRE) data support a transmembrane configuration of the peptide in the bilayers, but they also reveal that the system cannot be described by a single simple conformational model because there is a very high degree of dynamics and heterogeneity in the three-component system. To explore the origin of this heterogeneity and dynamics, we have compared the NOE and PRE data with MD simulations of an ensemble of alamethicin peptides in a DMPC bilayer. From all-atom MD simulations, the contacts between peptide, lipid, and water protons are quantified over a time interval up to 95 ns. The MD simulations provide a statistical base that reflects our NMR data and even can explain some initially surprising NMR results concerning specific interactions between alamethicin and the lipids.

1. Introduction

Antimicrobial peptides constitute a class of relatively short peptides, typically containing 10–50 residues with a high proportion of hydrophobic residues. Through antibiotic action they are part of the host-defense system in many living organisms, and the peptides are capable of killing, *inter alia*, Gram negative and Gram positive bacteria, even systems not amenable to conventional antibiotics.¹ This renders them of great interest as therapeutic agents and as potential alternatives to small-molecule antibiotics. With the increasing focus on antibiotic resistance the study of antimicrobial peptides becomes highly relevant from a pharmaceutical perspective. For most antimicrobial peptides only little is known of the exact mechanism. Many of the peptides are believed to disrupt the cell membrane, leading to cell lysis, while others are believed to interact with the immune system or the metabolism of the bacteria. With regard to their membrane disruption mechanism, several models have been put forward ranging from the formation of “barrel stave” ion channels,² toroidal pores (worm holes),³ and change of membrane properties by plastering the lipid surface with peptides in a “carpet action” model.⁴ Most

of the models are discussed in terms of a single mode of action, partly reflecting the structural biology approaches used for their characterization.

The objective of the present study is to analyze in more detail the dynamics and heterogeneity of antimicrobial systems at the atomic level. We use alamethicin as peptide target and mixed DMPC/DHPC (1,2-dimyristoyl-sn-glycero-3-phosphatidylcholine/1,2-dihexanoyl-sn-glycero-3-phosphatidylcholine) bicelles as lipid constituent. Our characterization methods are liquid-state NMR spectroscopy along with molecular dynamics (MD) simulations.

Alamethicin is a 20-residue peptide secreted by the fungus *Trichoderma viride*.⁵ The peptide belongs to the family of peptaibols which contains a high proportion of the helix-inducing aminoisobutyric acid (Aib) residue not belonging to the 20 standard amino acids. On average peptaibols contain 40% Aib residues.⁶ This also holds for alamethicin, which furthermore displays other peptaibol hallmarks such as an acetylated N-terminus and an amino alcohol in the C-terminus. Since the discovery of the ion conducting properties of alamethicin in the early 1970s⁷ and the X-ray structure of alamethicin by Fox and Richards⁸ in the early 1980s, alamethicin has been one of the most frequently studied models for antimicrobial peptides and larger ion channels.^{1,9} In the context of the present study, it is relevant to note that the high abundance of Aibs, with their lack of H^a protons, make peptaibols difficult to characterize structurally by NMR, in particular in a bicelle membrane

* To whom correspondence should be addressed. Tel.: +4589423841. Fax: +4586196199. E-mail: ncni@inano.dk.

[†] inSPIN, iNANO and Department of Chemistry, University of Aarhus.

[‡] Université du Maine.

[§] BiRC, University of Aarhus.

^{||} University of Illinois at Urbana–Champaign.

environment, which induces broad spectral lines due to slow molecular reorientation. This may explain why most NMR structural studies so far have addressed liquid-state NMR of alamethicin in organic solvents⁶ or solid-state NMR spectroscopy focusing on isotope-labeled alamethicin incorporated into oriented^{10–12} or nonoriented¹³ phospholipid bilayers. The latter studies, based on orientational constraints, suggest that alamethicin adapts a transmembrane configuration in bilayers at high concentrations, e.g., in a peptide:lipid molar ratio of 1:20.^{10–13} This interpretation is supported by oriented circular dichroism (OCD)¹⁴ and X-ray scattering studies.¹⁵ At lower concentrations, e.g., 1:100, or different hydration conditions, evidence exists that alamethicin adapts an orientation perpendicular to the membrane normal, interpreted as lying flat in the membrane surface, with the fraction of transmembrane to surface-oriented alamethicins depending in a sigmoidal fashion on the peptide concentration.^{14,16} A full atomic resolution structure of alamethicin forming a pore in a lipid bilayer based on experimental data has not yet been reported, while a barrel-stave model has been applied in MD simulations of alamethicin peptides incorporated in phospholipid bilayers.¹⁷

Returning to the objective of this paper, we will investigate in detail the incorporation of alamethicin into DMPC/DHPC bicelles by means of liquid-state NMR focusing on distance rather than angular/orientational type of structural information as obtained from previous solid-state NMR studies. Distance constraints were extracted from nuclear Overhauser enhancement spectroscopy (NOESY)¹⁸ and paramagnetic relaxation enhancement (PRE)¹⁹ experiments. The use of small DMPC/DHPC bicelles,^{20,21} rather than larger bilayers, ensures relatively fast reorientation of the peptide–lipid complexes effectively averaging anisotropic interactions to allow the acquisition of high-resolution ¹H NMR spectra. To cope with the heterogeneous and dynamical behavior of the system, we compare our experimental studies with MD simulations. The simulations describe atom by atom the diversity seen over time in a sample including several copies of the peptide, albeit on a small time scale compared to the NMR experiments. From the simulated diversity, average properties corresponding to NMR data can be extracted to support the interpretation of the experimental data.

2. Experimental Methods

Sample Preparation. Bicelle samples were prepared from 1 M stock solutions of 1,2-dimyristoyl-*sn*-glycero-3-phosphatidylcholine (DMPC) and 1,2-dihexanoyl-*sn*-glycero-3-phosphatidylcholine (DHPC) (ratio $q = 0.5$) in 10 mM phosphate buffer at pH 6.6. An appropriate volume of the DMPC/DHPC stock solution was first mixed with lyophilized peptide, which had been synthesized by solid-phase peptide synthesis.^{13,22} Phosphate buffer was added to yield a solution with 550 μ L total volume, 300 mM total lipid concentration, and 5 mM peptide. This implies a lipid concentration of 16% (w/v). For field lock, 10% D₂O was added. Finally, the solution was vortexed and centrifuged several times until the solution became clear. All lipids were obtained from Avanti Polar Lipids (Alabaster, AL). Most data presented in this work were acquired on native (not isotopically labeled) peptide in protonated lipids. A sample with partially ¹⁵N-amide labeled peptide (i.e., on 14 residues: Aib1, Aib3, Ala4, Aib5, Ala6, Aib8, Val9, Aib10, Gly11, Leu12, Aib13, Val15, Aib16, and Aib17), embedded in lipids with deuterated tails, was used in addition for assignment and establishment of additional structural constraints.

NMR Spectroscopy. All NMR data were acquired at a temperature of 308 K on a Bruker 700 MHz wide-bore Ultrashield Plus Avance-II spectrometer (16.4 T) using a triple resonance TXI probe or a Bruker 400 MHz wide-bore Avance spectrometer (9.4 T) using a double-resonance BBI probe, both equipped with a *z*-gradient. Data presented in this work were acquired by the following experiments: A 200 ms selective NOESY,¹⁸ acquired at 400 MHz with 96 transients and 256 increments. The final excitation pulse (EBURP2)²³ was selective for the frequency region of 6.7–8.9 ppm. For PRE experiments,¹⁹ the same pulse sequence was used with an additional inversion recovery period prior to the first pulse. A series of spectra was acquired at 700 MHz with 8 transients and 512 increments each. The recovery delays were set to 1, 200, 400, 600, 800, 1100, 1500, and 2500 ms. The spectrum with 1 ms delay was also used for additional identification of cross-peaks. The series was repeated after addition of 2 mM gadodiamide (Omniscan, Amersham, U.K.) to establish PRE information. The PRE data are presented as the differences in the two relaxation rates without any further scaling. A 150 ms 3D-NOESY-HSQC²⁴ at 700 MHz with 16 transients, 40 (¹⁵N) and 128 (¹H) increments. A STE-BP DOSY²⁵ at 400 MHz with 128 transients, 32 increments, $\delta = 4$ ms, and $\Delta = 1200$ ms. The spectra were processed using TopSpin (Bruker BioSpin, Rheinstetten, Germany), and analyzed with Sparky.²⁶ The extraction of relaxation parameters was done using NMRPipe.²⁷

Molecular Dynamics Simulations. The C monomer from the X-ray crystal structure of alamethicin crystallized from an acetonitrile/methanol solution⁸ (Protein Data Bank (pdb) file: 1AMT) was used for the system setup. The system was built from 25 peptides and 330 lipids. The helical peptides were placed strictly parallel to the membrane normal (the *z* axis) initially and only translated in the *xy* plane to form a 5×5 lattice, with the peptides' centers of masses separated in the *x* and *y* directions by 28.5 Å. With the peptides in place, a DMPC lipid molecule was replicated, randomly rotated around its long axis (*z*), and translated in the *xy* plane to fill the space between the peptides in the model. The lipid bilayer with the peptides was then solvated with water. The glutamate at position 18 was protonated, i.e., there are no charged residues present in alamethicin. Since the employed lipids are electroneutral, the system was electrically neutral and, thus, no counterions were needed. This setup is only expected to represent a situation where all alamethicin peptides are incorporated in the membrane environment in a transmembrane manner, since there is experimental evidence that at the peptide:lipid ratios used in the NMR experiments and in the MD simulations, this will be the favored orientation of the peptide.^{14,16}

The system (~125000 atoms) was energy-minimized and equilibrated for 200 ps with the peptides fixed. The peptides were then released and the entire system energy-minimized and equilibrated for 1 ns in the NPT ensemble ($T = 323$ K, $P = 1$ atm). The production run of 95 ns was carried out using the standard distribution of NAMD 2.6²⁸ and the CHARMM27 parameter set.²⁹ Periodic boundary conditions (PBC) were employed, but to avoid lipids entering the gel phase, the area of the unit cell was fixed at the value obtained at the end of the 1 ns equilibration in the NPT ensemble (120.5 Å × 123.7 Å). The pressure along the *z* direction was kept at 1 atm using the Nosé-Hoover Langevin piston³⁰ with a piston period of 100 fs and a decay time of 50 fs. The temperature was kept at 323 K using a Langevin thermostat with a damping coefficient of 0.5 ps⁻¹. van der Waals (vdW) interactions were cut off at 12 Å with shifting beginning at 10 Å to implement a smooth cutoff.

Electrostatic interactions were calculated using the particle mesh Ewald algorithm³¹ in the multiple time-stepping integration scheme, where interactions within 12 Å were considered short-range and evaluated each time step, while the long-range interactions were evaluated every fourth time step. Pair lists had a 14 Å cutoff and were updated at least once per 20 steps. The simulation was performed using a 1 fs time step.

Intermolecular proton–proton distances were inspected for the 25 alamethicin peptides in 40 snapshots spread evenly over the last 40 ns of the simulation. For proton pairs, where the average r^{-6} weighted distance was below 6 Å, the observed minimum and maximum values were used as restraints in the construction of the joint NMR–MD alamethicin structure.

Peptide–lipid and peptide–water contact maps were constructed on the basis of 100 snapshots spread evenly over the same 40 ns of the simulation. For selected alamethicin protons (all backbone amide protons, Gln7 and Gln19 amino protons, and Phl20 ring protons), the lipid protons or water oxygens within 15 Å were counted and weighted by r^{-6} , where r is the distance in angstroms between the alamethicin and lipid protons or alamethicin proton and water oxygen.

3. Results and Discussion

Size of the Peptide/Lipid Bicelles. DMPC/DHPC bicelles with a ratio $q = [\text{DMPC}]/[\text{DHPC}] = 0.5$ are expected to assume a disk-shaped form,³² in which the DHPC molecules form the rim, while the central part is mainly composed of a DMPC bilayer.^{21,33} The diameter of a bicelle is roughly 100 Å, although reported with a high uncertainty, while the thickness is about 50 Å.³³ We note that small deviations from this rim vs central part distribution of the lipids has been subject to discussions,³⁴ although under the conditions used in the present study, it is not believed to influence our data interpretation appreciably. We did not observe any DMPC–DHPC NOE contacts which could indicate significant deviations from the ideal DMPC-central DHPC-rim model. From X-ray scattering of a stack of oriented DMPC bilayers an average area per DMPC lipid was found as $60.6 \pm 0.5 \text{ Å}^2$ at 30 °C,³⁵ which allows 260 DMPC molecules per bicelle with a mass of 176 kDa without rim and about 427 kDa with DHPC rim. An alamethicin:DMPC ratio of 1:20 allows statistically 13 peptide molecules (26 kDa) per bicelle, yielding an overall mass of 453 kDa. The actual size of the bicelle in the solution may be determined by NMR diffusion (“DOSY”) experiments.²⁵ Following the model of Ortega and García de la Torre (eq 16 in ref 36), we can expect for a disk with the above dimensions a diffusion coefficient $D = 4.7 \times 10^{-11} \text{ m}^2/\text{s}$ at 308 K. By means of DOSY experiments, we found a diffusion coefficient of $D = (3.6 \pm 1) \times 10^{-11} \text{ m}^2/\text{s}$ measured at signals from both lipids and the peptide, verifying that large bicelles of the expected size are formed and that alamethicin is incorporated into them. We do not see any evidence for the formation of DHPC micelles from our spectra.

A rigid molecule with a molecular mass of 453 kDa would make the observation of NMR signals with liquid-state NMR techniques difficult. An amide proton in a particle with the corresponding rotational correlation time of $\tau_c = 150 \text{ ns}$ would be estimated to have a line width of about 200 Hz (approximated as an isotropic tumbler). In contrast, we observed, for example, a line width of $\Delta\Omega_{\text{fwhm}}/2\pi = 21 \text{ Hz}$ for H^N of Leu12 at 700 MHz, while the lipid signals are even significantly narrower; the resonances from the choline methyl groups, for example, display a line width of only 3.4 Hz (see Table 1). Accordingly, the bicelle cannot be considered as a rigid molecule, but there is a high degree of dynamics for the molecules in the membrane,

TABLE 1: Typical ^1H Line Widths Observed for Selected Signals of Alamethicin-Containing DMPC/DHPC Bicelles ($q = 0.5$) at 700 MHz

		$\Delta\Omega$ [2π Hz]		$\Delta\Omega$ [2π Hz]
Aib1	H^N	17	Gln19	H^ϵ
Leu12	H^N	21	Phl20	H^ζ
Aib13	H^N	23	lipid ^a	$(H_3\text{C})_3\text{N}$
Gln7	H^ϵ	14		

^a The choline methyl signal stems from both DHPC and DMPC. The line width is defined as full width at half-height (FWHH).

in particular rotational diffusion around the bilayer normal,³⁷ which leads to averaging of anisotropic interactions and thus narrowing of the lines. This rotational motion is obviously more pronounced for the smaller lipids than for the peptide molecules. Furthermore, the phenylalaniol (Phl20) ring may flip sufficiently fast³⁸ that the lines of the ring protons are much sharper than those of the other peptide signals (compare also Figure 3). Table 1 lists some representative line widths for different ^1H signals at 700 MHz. In our experiments these values, however, varied from sample to sample.

Structure. Relative to conventional liquid-state NMR protein structural investigations, the study of alamethicin in bicelles in the liquid phase is handicapped by several problems: (i) As stated above, due to the size of the bicelle/peptide complex, the lines are relatively broad. The ^1H coherences relax very fast, which, in particular, impedes the use of standard experiments for assignment through J couplings, such as COSY or TOCSY, and 3D derivatives of these (on the other hand, the size of the bicelles renders NOE transfers between neighboring protons very efficient). (ii) The absence of H^α protons and NMR-resolvable side-chain protons in the eight Aib residues reduces the number of NOEs, which are necessary as structural constraints. Instead, each Aib contains two methyl groups with low spectral dispersion: all of which are found in a narrow range of 0.05 ppm around 1.52 ppm. Only very few of them allow the unambiguous identification of interresidual cross-peaks. In addition, two residues are prolines, lacking amide protons. (iii) The excess of lipids in a ratio of 60:1 with respect to peptides makes the II and III quadrants of a ^1H 2D spectrum inaccessible for analysis of peptide resonances. This effect is enhanced by the higher peak intensity due to the smaller line width of the lipid signals (vide supra). Unless it is possible to take special precautions (in particular selective excitation before acquisition of the signal), the receiver gain often has to be reduced, compromising the attainable dynamical range and signal-to-noise ratio. DHPC and DMPC are commercially available in a partially deuterated form in which, however, only the tail protons are replaced. Even with the use of these lipids, there are residual ^1H signals of the other lipid protons that are as intense as the peptide signals. Furthermore, the use of deuterated lipids eliminates the possibility of obtaining lipid–peptide correlation signals. (iv) A precise determination of residual dipolar ^1H – ^{15}N couplings (RDC) is not possible. RDC would be very well suited for answering questions concerning the orientation of the peptide in the lipid bilayers, and they could in principle be measured in partially aligned membrane particles. However, due to the size of the particles, cross-correlation rates are very high, which leads to extreme broadening (50 Hz) with corresponding sensitivity loss of the anti-TROSY peak. Sørensen and co-workers³⁹ have developed techniques for more precise determination of RDC in bigger molecules, but the bicelles under investigation in our study exceeded the size amenable to experiments even with these methods. (v) It turns out that the

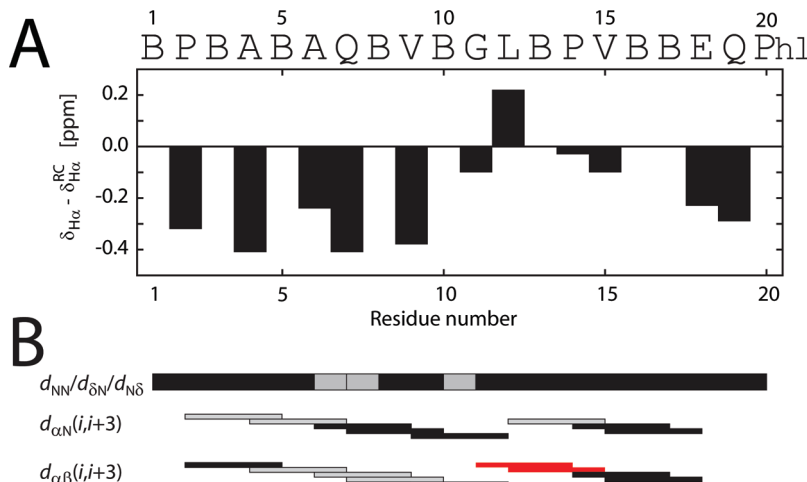


Figure 1. Compilation of NMR information on the structure of alamethicin in DMPC/DHPC bicelles. (A) H^α chemical shift index. (B) NOE connectivities. Black connectors: NOEs observed for at least one of the indicated types. Gray: NOEs ambiguous due to overlap. Red: NOEs missing. No connector: no NOE possible.

system “peptide in a bicelle” cannot be represented by a rigid model, in which intermolecular distances and orientations have a constant value.

Analysis of the H^α chemical shifts can give a good indication of the secondary structure.⁴⁰ Overall it is seen that the H^α chemical shifts of the alamethicin residues are predominantly lower than their respective random coil values. The only exception is residue Leu12, which has a H^α chemical shift 0.2 ppm higher than the random coil value. Hence, the overall secondary chemical shift pattern (Figure 1A) indicates an α -helical structure which is broken/bent in the vicinity of residue Leu12, in agreement with previous X-ray diffraction (XRD), solid-state NMR, and MD interpretations.^{8,10,41} In addition, we note that the outlier Leu12 is located in the helix kink inducing Gly-X-X-Pro motif of Gly11 and Pro14. The second source of secondary structure information is the appearance and intensity of cross-peaks in NOESY spectra, as shown in Figure 1B. The presence of medium-range NOE connectivities $d_{\alpha\text{N}}(i,i+2)$, $d_{\alpha\text{N}}(i,i+3)$, $d_{\alpha\text{N}}(i,i+4)$, and $d_{\alpha\beta}(i,i+3)$ is normally used to confirm an α -helical structure. Due to the high abundance of Aib and Pro amino acids, several of these NOEs do not exist a priori or could not be assigned unambiguously (labeled gray in Figure 1B). Only for the residues Gly11 and Leu12, NOEs that would have been observed for a helical structure were missing. Thus, the existence and absence of medium-range NOEs corroborate the observed H^α chemical shifts, indicating a broken/bent α -helical structure. No long-range or intermolecular NOEs could be confirmed. Thus, on the basis of these data, we cannot make any conclusions on a potential oligomeric arrangement. A structural model of alamethicin in bicelles was calculated by doing a simulated annealing with CNS⁴² (see Figure 2) using 181 distance restraints from NMR and 925 hydrogen–hydrogen distances from the MD simulations. The model fulfills all except one of the 181 distance restraints from NMR. All hydrogen–hydrogen distances in the model are within the minimum/maximum distances from the MD simulations.

Lipid–Peptide Connectivities Observed by Liquid-State NMR. In addition to the intermolecular alamethicin cross-peaks, the NOESY spectra reveal NOE cross-peaks between alamethicin and the most dominant lipid signals, while cross-peaks to the less dominant lipid signals are virtually absent in the spectra. This may be ascribed to the heterogeneity of the involved intermolecular connectivities and the motion of the peptide and lipid molecules with respect to each other. The

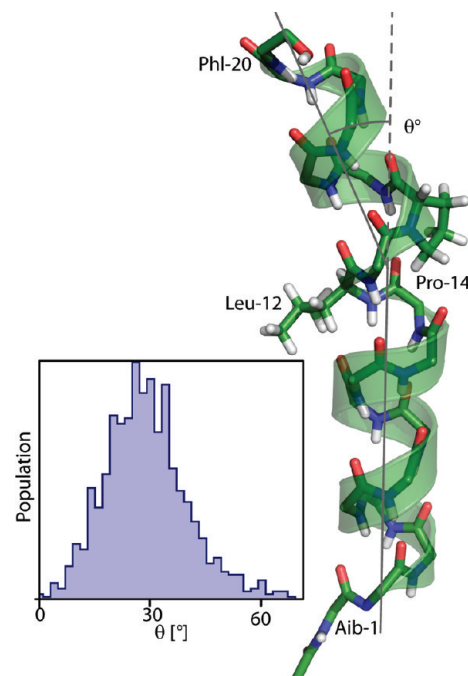


Figure 2. Structural model of alamethicin in bicelles calculated on the basis of NMR and MD restraints using simulated annealing in CNS. The kink in this model is 31°. The distribution of kink angles from the MD simulations is indicated in the insert (bin size, 2°). The NMR data consistently indicate the existence of the kink, but do not allow, however, an estimate of its size.

most prominent examples of observable lipid–peptide connectivities are a row of cross-peaks of—as far as resolvable—all alamethicin resonances between 6.5 and 9 ppm with a signal from the acyl chain of DMPC at 1.28 ppm (Figure 3A). Only the first and second CH_2 groups of the lipid acyl chains as well as the terminal methyl group are separated;³² all other acyl groups (positions 4–13) are degenerated to this one resonance at 1.28 ppm. The corresponding DHPC peak at 1.30 ppm can be distinguished by means of a TOCSY experiment (not shown).

Figure 3A shows an excerpt of a NOESY spectrum of this region, and Figure 3B shows the cross-section of this spectrum at the DMPC acyl resonance compared to a standard 1D spectrum. All peptide signals show cross-peaks, including those stemming from the termini. Those, H^N of Aib1, Glu18,

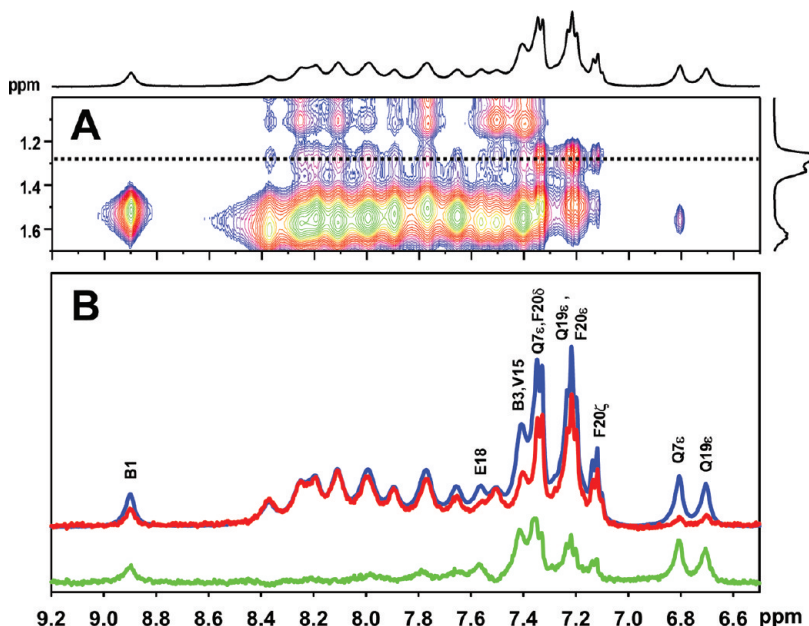


Figure 3. (A) Excerpt from a 200 ms NOESY spectrum of alamethicin in bicelles showing cross-peaks to the acyl chain $C^{4-13}H_2$ protons of DMPC labeled by the dotted bar. (B) Cross-section of the NOESY spectrum in A at the frequency of the DMPC acyl resonances $C^{4-13}H_2$ (1.28 ppm, red) in comparison with a 1D spectrum (blue). The cross-section is scaled such that no peak is higher than for the 1D spectrum. The difference spectrum is colored green.

and as far as resolvable the peaks of Phe20 are, however, reduced. The same applies for the amino signals of Gln7 and Gln19 at 6.7 and 6.8 ppm. This reduction is not due to deleterious effects during the pulse sequence such as water exchange or different relaxation during the 200 ms mixing time; it is also present if one takes the diagonal peaks as a reference (relative peak intensities are then for example as follows: Aib1, 0.03; Aib13, 0.14). Further resolvable intermolecular cross-peaks were found between the methyl groups of the choline headgroup of the lipids on the one side and the H^N of Aib1 as well as the ring protons H^δ and H^ϵ of the terminal Phe20 on the other side. In addition, the Phe20 ring protons also seem to show cross-peaks (albeit very small) to the methyl group of DHPC, indicating that the bicelle does not perfectly mimic a membrane double layer.

Figure 4 sums up the observed alamethicin–lipid cross-peaks within a sketch of alamethicin and lipid molecules. Overall, the cross-peak pattern supports a transmembrane insertion of alamethicin into the bicelle with some deviations to be discussed later. We note that the weak NOE of the termini to the acyl groups cannot be explained by an in-plane orientation in the bicelle.

Lipid–Peptide Contacts Quantified by Molecular Dynamics Simulations. With the aim of exploring in more detail the flexibility of the alamethicin–lipid interactions and to provide a statistical basis for understanding the observed (and not observed) alamethicin–lipid cross-peaks, we conducted molecular dynamics simulations of alamethicin in a DMPC bilayer using a setup similar to that described recently.⁴¹ The MD simulations describe the dynamics of an ensemble (or distribution) of alamethicin structures with more or less transmembrane orientation. From the atomic details of the simulation both qualitative and quantitative observations can be deduced that compare to or complement the NMR results.

To extract quantitative information from the MD simulations that directly relate to our NMR data, lipid–peptide “contacts” were counted over the last 40 ns of a 95 ns simulation. For each of the selected alamethicin peptide protons, in 25 peptides

in 100 snapshots, the number of lipid protons nearby was counted with the distance weight r^{-6} to mimic the intensity of NOE cross-peaks. Contributions from lipid protons further away than 15 Å are insignificant and are therefore not considered. The weighted contact counts are grouped for lipid protons that cannot be distinguished in NMR, either because they are equivalent or because the signals are joint (see Table 2). In this manner the counts can be compared directly with the normalized cross-peak intensities in our NOESY spectra. In agreement with our NOESY spectra, the interactions with the acyl chain protons (C_4-C_{13}) form the majority of the contact counts due to the large number of protons involved. The tail methyl and the NMR-distinguishable C^2H_2 and C^3H_2 give, as groups of two to three protons, only few counts, and accordingly no NOE cross-peaks were detected in the experiment. Separating the acyl chain contact counts according to the positions in the tails reveals the expected distribution for a transmembrane orientation: while the central Gly11 H^N has the most counts with $C^{12}H_2$ and $C^{13}H_2$ in the middle of the bilayer, the peptide H^N of both termini (i.e., Aib1, Aib3, Ala4, Glu18, Gln19, and Phe20) have the highest counts with C_2 and C_3 , which are not included in the NMR acyl resonance, and with the headgroup. Consistently, the experimental NOE cross-peaks involving the resonances of many of the terminal H^N (Aib1, Aib3 (and/or Val15, not resolvable), Glu18, and potentially Phe20, which is overlapping with the other Phe20 resonances) with the main acyl tail peak ($C^4H_2-C^{13}H_2$) are relatively weak, as seen in Figure 3. The same comparison holds for the ring protons of Phe20, which has still high counts from $C^4H_2-C^{13}H_2$ in the MD simulations and strong cross-peaks in the NMR spectra, but when taking the 1D spectrum as a reference (see Figure 3), they are weakened. The amino group signals of Gln7 and Gln19 are particularly weakened. This is only partially reflected in the simulation: the sums of Gln7 and Gln19 side-chain contacts with the acyl chain $C^4H_2-C^{13}H_2$ belong to the highest (as we do not see it in NMR); however, there is an emphasis of the polar side chains on contact counts with the outer lipid protons. The geometrically expected

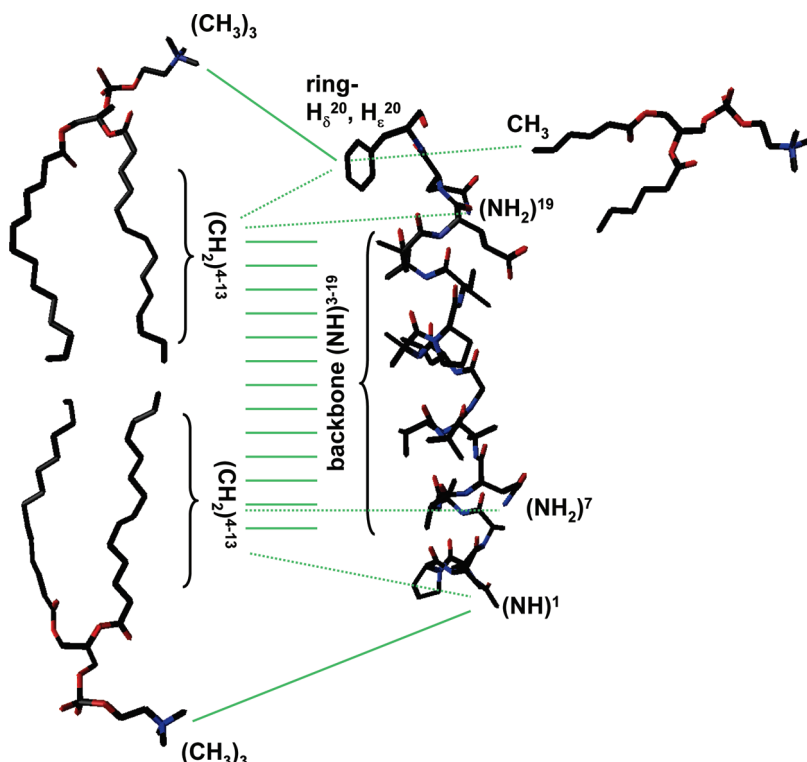


Figure 4. Summary of observed NOE connectivities between alamethicin and lipid molecules as illustrated by lines between the involved structural elements of the individual molecules: left, DMPC; middle, alamethicin; right, DHPC. The NOE are between the associated protons rather than heavy atoms shown in this scheme for the sake of visual clarity. Relatively weak cross-peaks are denoted by dotted lines.

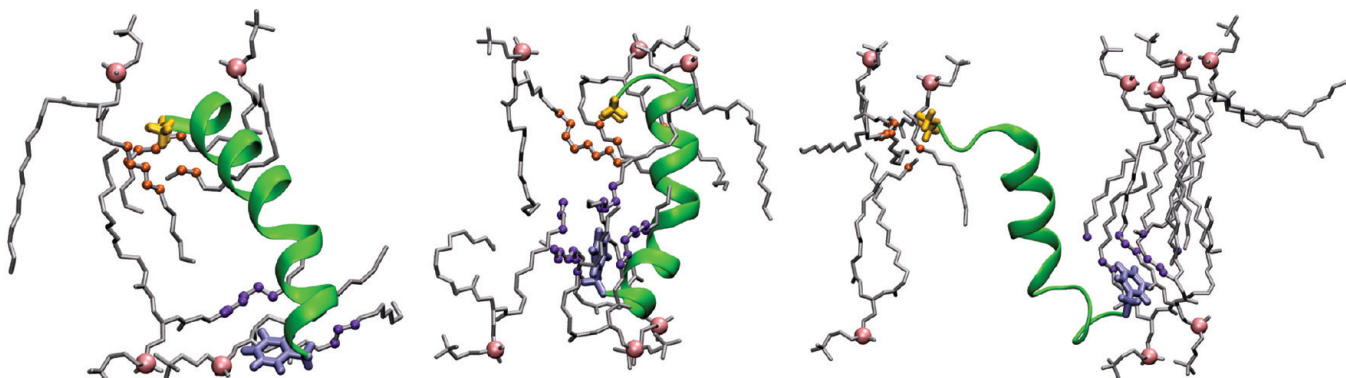


Figure 5. Representative lipid-peptide contacts obtained from MD simulations. The three snapshots illustrate the diversity of the lipid-peptide connectivities emphasizing contacts between the N- and C-terminal peptide residues with the lipid chains. Selected peptide(s) from Figure 9C are shown in green ribbon with Aib1 in yellow licorice and Phl20 in ice-blue licorice. Only lipids having acyl C4–13 carbons within 5 Å of Aib1 or Phl20 are shown, phosphors are shown as pink spheres, and hydrogens are omitted for clarity. The C4–13 carbons within 5 Å are shown as orange spheres for Aib1 and purple spheres for Phl20.

higher propensity of side-chain protons for contacts to lipids is reflected in the simulations, but not in the NMR data.

The other comparable set of information extracted from MD simulations and NMR NOE measurements is the contact counts between the methyl groups of phosphocholines and the peptides. Not surprisingly, the ring of Phl20 displays some of the highest counts, which is also reflected by cross-peaks to the Phl20 ring protons H_δ and H_ϵ . Other cross-peaks of the phosphocholine CH_3 to the Gln7 and Gln19 amino groups were, however, not unambiguously detectable. For the N terminus, the highest choline contact counts are to the amide protons of Aib1 and Aib3—the former of which is confirmed by the only other cross-peak to the headgroup methyl signal. Cross-peaks to the DMPC tail terminal methyl groups could not be observed, although they have relatively high contact counts in the MD simulations. Representative snapshots from MD simulations illustrating the

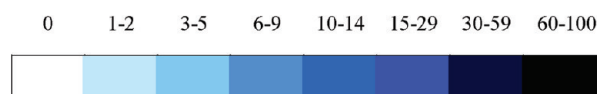
diversity of the lipid-peptide interactions with particular focus on contacts to the N- and C-terminals of the peptide are shown in Figure 5.

Although a perfect (one-to-one) match between the results of the MD simulations and NMR NOE data is not expected nor achieved, they reflect tendencies. Most importantly, they both give indications of the fluid nature of the membrane environment and emphasize that NMR observations cannot be interpreted in terms of a simple model where one body (the peptide) is incorporated into a bigger body (the bilayer), but rather a model where it is dissolved in the bilayer. Furthermore, we note that not all potential cross-peaks may be visible in the experimental NMR spectra, some might be hidden by spectral overlap.

Paramagnetic Relaxation Enhancement. Paramagnetic relaxation enhancement studies may be conducted using ga-

TABLE 2: Peptide–Lipid Contacts Determined by the MD Simulations^a

	Cho CH ₃	Acy C2	Acy C3	C3	C5	C6	C7	C8	C9	C10	C11	C12	C13	Acy C4-13	Acy CH ₃
Aib1	2	3	3	2	2	1	1	1	1	1	0	0	1	10	2
Aib3	2	1	1	1	1	1	0	0	0	0	0	0	0	3	0
Ala4	1	1	1	1	1	1	0	0	0	0	0	0	0	4	1
Aib5	1	1	1	1	1	1	1	1	1	1	0	1	1	7	1
Ala6	1	1	1	1	1	1	1	1	1	1	1	1	1	9	2
Gln7	0	1	1	1	1	1	1	1	1	1	1	1	1	7	1
Aib8	0	1	1	1	1	1	1	1	1	1	1	1	1	11	2
Val9	0	0	0	1	1	1	1	1	1	1	1	1	2	10	3
Aib10	0	1	1	1	1	1	1	1	1	1	2	2	2	14	3
Gly11	0	1	1	1	1	1	2	2	2	2	3	3	3	20	4
Leu12	0	0	0	0	0	1	1	1	1	1	2	2	2	12	4
Aib13	0	0	0	0	0	1	1	1	1	1	1	1	1	9	3
Val15	0	1	1	1	1	1	1	1	1	1	1	1	1	9	2
Aib16	0	0	0	1	1	1	1	1	1	1	1	1	1	7	2
Aib17	0	1	1	1	1	1	1	1	1	1	1	1	1	10	2
Glu18	1	2	1	1	1	1	1	1	0	0	0	0	1	6	1
Gln19	1	1	1	1	1	0	0	0	0	0	0	0	0	4	1
Phl20	2	1	1	1	1	0	0	0	0	0	0	0	0	4	1
Gln7ε	9	14	13	10	6	6	4	3	2	2	2	2	3	40	9
Gln19ε	15	12	13	10	7	8	6	4	4	3	3	3	4	51	9
Phl20δ	12	10	9	8	8	7	6	5	4	4	3	3	4	53	7
Phl20ε	12	14	14	13	13	12	11	10	9	8	8	8	9	100	17
Phl20ζ	4	8	12	10	9	9	7	6	5	4	3	3	4	61	8



^a The values represent the relative number of occurrences that a peptide proton (H^N , unless specified otherwise) is situated within a radius $r < 15 \text{ \AA}$ of a lipid proton (group), weighted by r^{-6} . The contacts are counted over the last 40 ns of the 95 ns simulation. The column Acy C4–13 is the sum over the preceding columns C4–C13, for better comparison with the experimental NOE data. Cho CH₃ designates the choline methyl groups.

dodiamide (Gd(DTPA-BMA)), a gadolinium complex that, in contrast to other paramagnetic probes, remains in solution. It has been developed as a contrast agent (brand name Omniscan) for magnetic resonance imaging (MRI) and does not bind to any peptide sites or lipids.⁴³ This property renders gadodiamide useful to determine the (average) immersion depth of regions of alamethicin in the DMPC/DHPC bicelles. In the absence of gadodiamide, the longitudinal relaxation rates R_1 of the protons of alamethicin lie in the range of $0.8\text{--}1.7 \text{ s}^{-1}$. The addition of 2 mM gadodiamide enhances R_1 of all protons of alamethicin by $0.1\text{--}2 \text{ s}^{-1}$. The enhancement is expected to be high for protons that are close or even exposed to the solvent phase and decays with the distance from the surface. In the ideal case, the PRE decreases with the third power of the distance d of a proton from an ideal water/lipid interface.⁴⁴ In Figure 6A, this is shown by mapping the bicelle lipid PREs to structural models of DHPC and DMPC. While the headgroup choline methyl group has an enhancement of 1.4 s^{-1} , the acyl C²H₂ protons close to the

headgroup show 0.4 s^{-1} , and the terminal tail methyl group in the middle only 0.1 s^{-1} .

In parts B and C of Figure 6, the peptide PREs are mapped to a structural model of alamethicin. The protons at the termini have relatively high PRE, where the enhancement takes values of $0.4\text{--}0.6 \text{ s}^{-1}$ for many protons of the three terminal residues. A particularly strong enhancement is found for the acyl group attached to Aib1 (0.9 s^{-1}), which accordingly seems to have a relatively high exposure to the solvent, while the effect is less pronounced for the phenyl ring of Phl20 and the residue Pro2. The backbone in Figure 6C shows the effect only for the amide protons, which are more comparable than the side-chain protons and few outlying side-chain protons. The finding is so far consistent with a model of a transmembrane insertion of alamethicin in bicelles. However, the PRE does not show a monotonous decay toward the expected middle of the membrane around residue number 10. In contrast, the rate in the inner part (i.e., residues 4–16, $0.1\text{--}0.3 \text{ s}^{-1}$) does not show any further

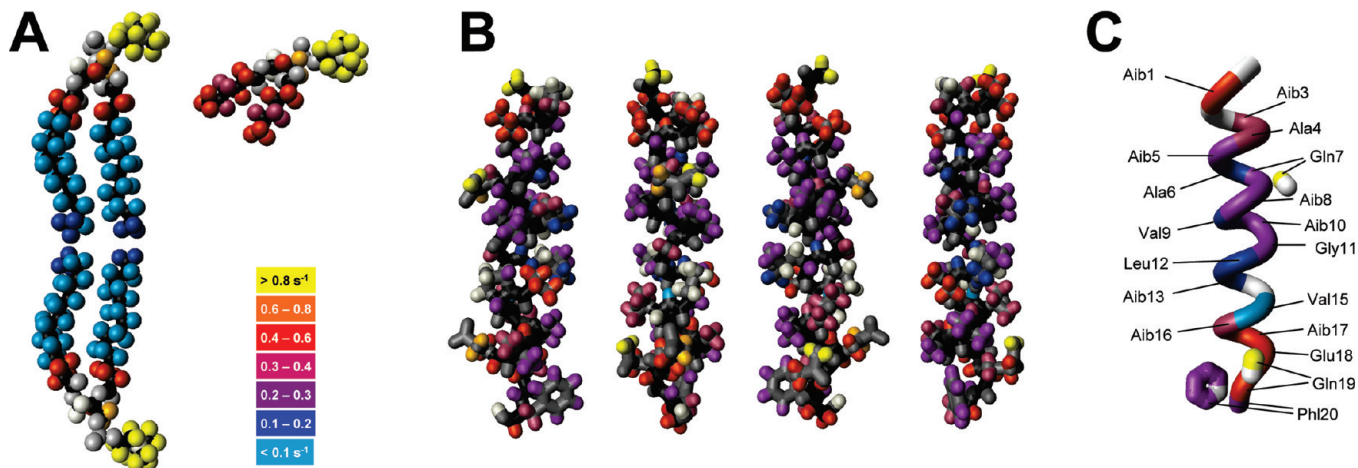


Figure 6. Matching of the proton paramagnetic relaxation enhancements (PRE) to structural models of (A) DMPC (left) and DHPG (right), (B) alamethicin, as seen from different perspectives (model turned by 0, 90, 180, and 270°), (C) alamethicin, representation reduced to the enhancements that are compared with the MD simulation, i.e., H^N (represented by the backbone position), ring protons, and side-chain H_2N signals. Different colors represent different enhancements of the longitudinal relaxation rate. Protons labeled in light gray in A and B do not allow a reliable determination of the relaxation rate, mostly due to spectral overlap. Dark gray and black spheres designate all nonproton atoms.

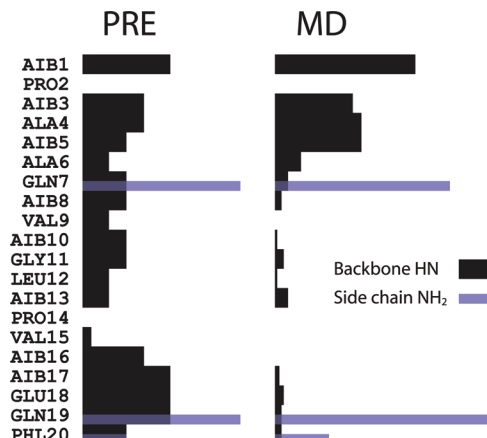


Figure 7. Peptide–water contact table of the MD simulations in comparison with PRE data. The bars in the MD part represent the relative number of occurrences that a peptide proton (backbone H^N or side chain H_2N) is situated within a radius $r < 15 \text{ \AA}$ of a water molecule, weighted with r^{-6} . The contacts are counted over an interval of 40 ns. The length of the bars in the left part is proportional to the paramagnetic relaxation enhancement in s^{-1} and corresponds to Figure 6B,C.

gradient. Moreover, the exposed (in a free molecule) $C^{\prime}H_2$ groups of the polar residues Gln7, Glu18, and Gln19 ($0.4\text{--}0.6 \text{ s}^{-1}$) and particularly the amino groups of the two glutamines ($0.9\text{--}1.8 \text{ s}^{-1}$) show particularly strong enhancements. While it is conceivable that the polar side chain of Gln19 orients toward the water interface, the high rate for Gln7 is on the first glance surprising; as in a simple geometrical transmembrane model it is buried in the middle of the membrane. These PRE findings of the three polar side chains would therefore rather speak for an in-plane orientation of alamethicin in the membrane, with the polar groups oriented out of the surface. Such an interpretation would, however, be in contradiction with the previous interpretations of PRE and NOE data, which both showed features of the termini that point to a transmembrane orientation.

A possible way to overcome this dilemma would be to assume the formation of a pore, which is already an established structural model for alamethicin in a different membrane environment by means of single-channel recordings.^{2,45} A hexameric pore, the favored model,⁴⁶ would however be too small for a gadodiamide complex to enter. The inner diameter of such a pore would be

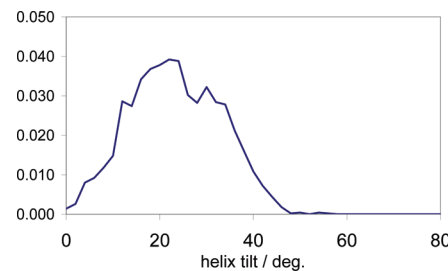


Figure 8. Distribution of the helix orientation with respect to the membrane normal from the same snapshots of the MD simulations as used for Table 2 and Figure 7. The counts are scaled to the total number of counts, the increment being 2°.

about 8 \AA (a value that however depends much on the definition). This is the minimal size of the gadodiamide complex. Also, the Gd^{3+} ion is not expected to be able to leave the complex. We have performed PRE experiments with Dy^{3+} in solution to see the effect of a paramagnetic agent that can enter a potential pore, and we did not observe any noticeable difference to the gadodiamide results. A more plausible explanation for the high PRE of Gln7 would involve diffusion of paramagnetically relaxed water or spin diffusion into the pore. The assumption of a pore with the polar Gln7 and Glu18 side chain pointing preferably toward the center (Gln19 is turned by 90°), the relaxation of which being enhanced via pore water, would require further consequences in the PRE data. In this case, the PRE of residues on the pore side should be higher, which is however not observed (Figure 6B). In contrast, there is a tendency toward a radial distribution of the PRE effect, as one would expect in a free molecule in solution. Exposed side-chain protons have relatively higher PRE, while buried H^N are less influenced by the paramagnetic agent.

Water–Peptide Contacts in Molecular Dynamics Simulations. To mimic the PRE data, water–peptide contacts have been counted in our MD simulations in a manner similar to the NOE data described above. We did not simulate the single gadodiamide molecules, but rather consider them—as in the NMR PRE model—as homogeneously distributed in the water phase and count the water contacts instead. Also here, a distance weighting with r^{-6} has been used. The sum over all water contacts is supposed to mimic the r^{-3} dependence of the PRE on the distance from the lipid/water interface. All contacts within

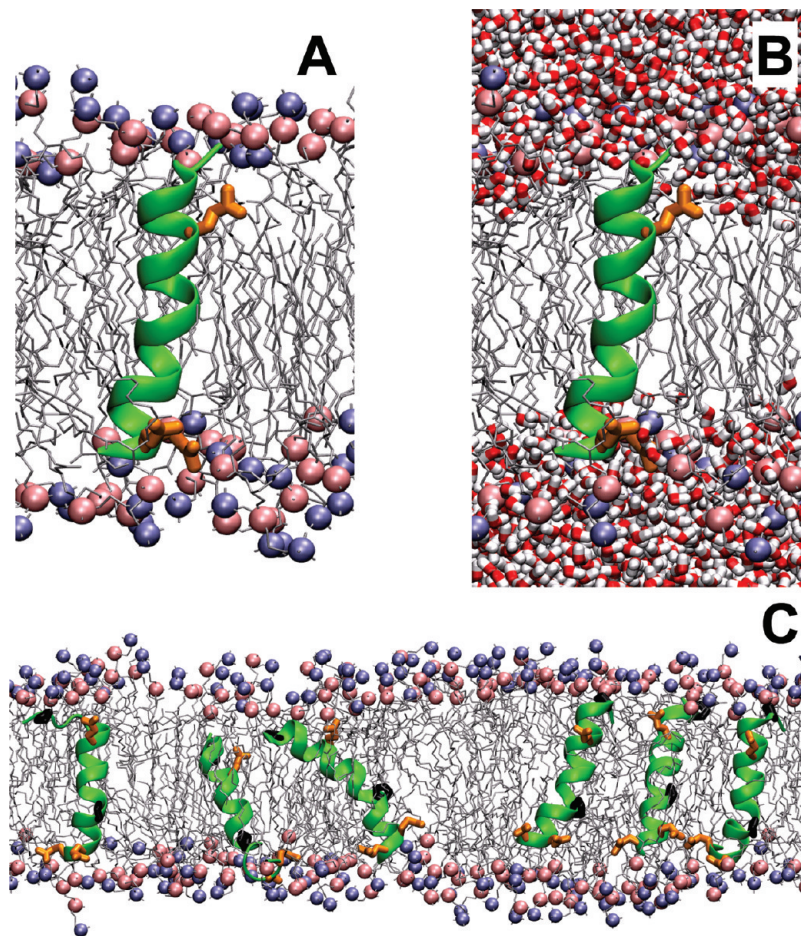


Figure 9. Snapshots from the MD simulations of alamethicin in a DMPC bilayer. The peptides are shown in green ribbon with the N-terminus in the top and the hydrophilic side chains of Gln7, Glu18, and Gln19 are shown in orange licorice. Lipids are colored gray with head groups labeled in blue (N) and pink (P). Panels A and B show the same snapshot, without and with the water molecules, respectively. (C) Illustration of the diversity of both the peptides and the lipids. Pro2 and Pro14 side chains are shown in black licorice.

$r = 15 \text{ \AA}$ have been counted; a convergence is, however, already achieved at $r = 5 \text{ \AA}$. Analogous to the PRE results, there are many contacts in the N-terminal region, there are however only a few in the C-terminus (Figure 7): only the polar Gln19 amino group and the Phe20 ring exhibit a large number of contacts with water. Striking is the high number of water contacts to the Gln7 amino group, which is in line with the previously discussed, unexpectedly high PRE for this group. This analogous observation in the contacts allows us to understand its basis by monitoring the underlying MD simulations. In the simulations, the peptides retain mostly their transmembrane orientations with tilt angles ranging between 10 and 35° with respect to the membrane normal (Figure 8), and they do not form pores in the membrane. The explanation for the high Gln7 amino PRE and MD counts can be found in Figure 9, showing a snapshot from the MD simulations: the polar group of Gln7 is oriented toward and making contacts with the headgroups of the lipids. This is not only an occasional state, but rather the preferred orientation of the Gln7 side chains. Moreover, water penetrates the headgroup region completely, even forming transient cavities in the tail region of the membranes, so that the NH_2 group of Gln7 is readily exposed to water. In terms of comparison with PRE data one has to take into consideration that gadodiamide is probably too big to diffuse into the headgroup region. However, as stated before, there is a strong relaxation enhancement of water, which is likely to be transferred via NOE or even exchange to the amino protons; the substitution of gadodiamide by smaller Dy^{3+} ions gave in principle the same

result. The diffusion of water molecules into the membrane as well as magnetization transfer via water has some implications on the analysis of PRE data. There is no clear water/lipid interface, to which a distance r can be defined. Therefore the r^{-3} model may need a distance correction term.

As the MD simulations are initialized—in accord with the principal NMR results—from a transmembrane orientation, they certainly have a bias to this conformation. During the 95 ns of the simulation run they do not leave the region of preferred helix tilt angles shown in Figure 8. In the simulations, we do not observe flips from a transmembrane orientation to an in-plane orientation as described by Bechinger et al.⁴⁷ Obviously we cannot completely exclude the existence of such processes as they could occur with a probability that is too low for our simulation time and with an in-plane population being too low to be seen by our NMR experiments. The transmembrane orientation model yields a consistent interpretation of the NMR and MD data.

4. Conclusions

Liquid-state NMR has provided specific information about the incorporation of peptides such as alamethicin into a membrane environment in two ways: (i) the direct proof of contacts between specific peptide protons and lipid protons via NOE and (ii) characterizing the immersion depth of particular peptide protons as the distance to the water phase as measured by PRE. Our NMR data overall indicate a transmembrane

incorporation of the peptide; the interpretation of some features is, however, not straightforward when assuming a simple rigid model of incorporation. MD simulations, however, show the fluid character of the membrane environment, in which the peptide is rather dissolved than incorporated, and that the location and orientation of the peptide molecules are consequently mobile and heterogeneous. By counting contacts from the peptide protons to the lipid or water protons, data sets are extracted from the simulations that can be compared with NOE or PRE results, respectively. The interpretation of the NMR data in conjunction with MD contact data gives a more consistent picture of the behavior of alamethicin as a flexible entity in the membrane environment with a preferential transmembrane configuration. We believe that our results shed new light on the flexible structures of antimicrobial ion channels and reveals that the combination of NMR spectroscopy and MD simulations may pave the way for further understanding and description of the assembly and action of such complex and highly dynamic systems.

Acknowledgment. This research was supported by grants from the Danish National Research Foundation, Carlsbergfondet, and Lundbeckfonden. The authors gladly acknowledge TeraGrid computer time allocation (MCA06N060), as well as computer time from the DoD High Performance Computing Modernization Program at the Arctic Region Supercomputing Center, University of Alaska at Fairbanks. We thank Dr. P. Vestergaard-Poulsen and his colleagues at Aarhus University hospital for providing us with gadodiamide.

References and Notes

- (1) Hancock, R. E.; Patryk, A. *Curr. Drug Targets Infect. Disorder* **2002**, *2*, 79–83.
- (2) Brogden, B. A. *Nat. Rev. Microbiol.* **2005**, *3*, 238–250.
- (3) Hamill, P.; Brown, K.; Jenssen, H.; Hancock, R. E. *Curr. Opin. Biotechnol.* **2008**, *19*, 628–636.
- (4) Baumann, G.; Mueller, P. J. *Supramol. Struct.* **1974**, *2*, 538–557.
- (5) Ludtke, S. J.; He, K.; Heller, W. T.; Harroun, T. A.; Yang, L.; Huang, H. W. *Biochemistry* **1996**, *35*, 13723–13728.
- (6) Pouy, Y.; Rapaport, D.; Mor, A.; Nicolas, P.; Shai, Y. *Biochemistry* **1992**, *31*, 12416–12423.
- (7) Meyer, C. E.; Reusser, F. *Experientia* **1967**, *23*, 85–86.
- (8) Whitmore, L.; Wallace, B. A. *Eur. Biophys. J.* **2004**, *33*, 233–237.
- (9) Gordon, L. G.; Haydon, D. A. *Biochim. Biophys. Acta* **1972**, *255*, 1014–1018.
- (10) Fox, R. O.; Richards, F. M. *Nature* **1982**, *300*, 325–330.
- (11) Hall, J. E.; Vodyanoy, I.; Balasubramanian, T. M.; Marshall, G. R. *Biophys. J.* **1984**, *45*, 233–247.
- (12) Bak, M.; Bywater, R. P.; Hohwy, M.; Thomsen, J. K.; Adelhorst, K.; Jakobsen, H. J.; Sørensen, O. W.; Nielsen, N. C. *Biophys. J.* **2001**, *81*, 1684–1698.
- (13) Vosegaard, T.; Bertelsen, K.; Pedersen, J. M.; Thøgersen, L.; Schiøtt, B.; Tajkhorshid, E.; Skrydstrup, T.; Nielsen, N. C. *J. Am. Chem. Soc.* **2008**, *130*, 5028–5029.
- (14) Salnikov, E. S.; Friedrich, H.; Li, X.; Bertani, P.; Reissmann, S.; Hertweck, C.; O’Neil, J. D. J.; Raap, J.; Bechinger, B. *Biophys. J.* **2009**, *96*, 86–100.
- (15) Bertelsen, K.; Pedersen, J. M.; Rasmussen, B. S.; Skrydstrup, T. S.; Nielsen, N. C.; Vosegaard, T. *J. Am. Chem. Soc.* **2007**, *129*, 14717–14723.
- (16) Chen, F.-Y.; Lee, M.-T.; Huang, H. W. *Biophys. J.* **2002**, *82*, 908–914.
- (17) Constantin, D.; Brotons, G.; Jarre, A.; Salditt, T. *Biophys. J.* **2007**, *92*, 3978–3987.
- (18) Huang, H. W.; Wu, Y. *Biophys. J.* **1991**, *60*, 1079–1087.
- (19) You, S. C.; Peng, S. Y.; Lien, L.; Breed, J.; Sansom, M. S. P.; Woolley, G. A. *Biochemistry* **1996**, *35*, 6225–6232.
- (20) Berendsen, H. J. C.; Sansom, M. S. P. *Biophys. J.* **1999**, *76*, 1757–1769.
- (21) Tieleman, D. P.; Hess, B.; Sansom, M. S. P. *Biophys. J.* **2002**, *83*, 2393–2407.
- (22) Zhu, Q.; Vaughn, M. W. *J. Phys. Chem. B* **2005**, *109*, 19474–19483.
- (23) Jeener, J.; Meier, B. H.; Bachmann, P.; Ernst, R. R. *J. Chem. Phys.* **1979**, *71*, 4546–4563.
- (24) Kosen, P. A. *Methods Enzymol.* **1989**, *177*, 86–121.
- (25) Sanders, C. R.; Schwonek, J. P. *Biochemistry* **1992**, *31*, 8898–8905.
- (26) Lee, D.; Walter, K. F. A.; Brückner, A.-K.; Hilty, C.; Becker, S.; Griesinger, C. *J. Am. Chem. Soc.* **2008**, *130*, 13822–13823.
- (27) Hjørringgaard, C. U.; Pedersen, J. M.; Vosegaard, T.; Nielsen, N. C.; Skrydstrup, T. *J. Org. Chem.* **2009**, *74*, 1329–1332.
- (28) Geen, H.; Freeman, R. *J. Magn. Reson.* **1991**, *93*, 93–141.
- (29) Montelione, G. T.; Lyons, B. A.; Emerson, S. D.; Tashiro, M. *J. Am. Chem. Soc.* **1992**, *114*, 10974–10975.
- (30) Morris, K. F.; Johnson, S. S. *J. Am. Chem. Soc.* **1992**, *114*, 3139–3141.
- (31) Goddard, T. D.; Kneller, D. G. *SPARKY 3*; University of California: San Francisco.
- (32) Stejskal, E. O.; Tanner, J. E. *J. Chem. Phys.* **1965**, *42*, 288–292.
- (33) Delaglio, F.; Grzesiek, S.; Vuister, G. W.; Zhu, G.; Pfeifer, J.; Bax, A. *J. Biomol. NMR* **1995**, *6*, 277–293.
- (34) Phillips, J. C.; Braun, R.; Wang, W.; Gumbart, J.; Tajkhorshid, E.; Villa, E.; Chipot, C.; Skeel, R. D.; Kale, L.; Schulten, K. *J. Comput. Chem.* **2005**, *26*, 1781–1802.
- (35) MacKerell, A. D.; Bashford, D.; Bellott, M.; Dunbrack, R. L.; Evanseck, J. D.; Field, M. J.; Fischer, S.; Gao, J.; Guo, H.; Ha, S.; Joseph-McCarthy, D.; Kuchnir, L.; Kuczera, K.; Lau, F. T. K.; Mattos, C.; Michnick, S.; Ngo, T.; Nguyen, D. T.; Prodhom, B.; Reiher, W. E.; Roux, B.; Schlenkrich, M.; Smith, J. C.; Stote, R.; Straub, J.; Watanabe, M.; Wiorkiewicz-Kuczera, J.; Yin, D.; Karplus, M. *J. Phys. Chem. B* **1998**, *102*, 3586–3616.
- (36) Feller, S. E.; Zhang, Y. H.; Pator, R. W.; Brooks, B. R. *J. Chem. Phys.* **1995**, *103*, 4613–4621.
- (37) Darden, T.; York, D.; Pedersen, L. *J. Chem. Phys.* **1993**, *98*, 10089–10092.
- (38) Vold, R. R.; Prosser, R. S.; Deese, A. J. *J. Biomol. NMR* **1997**, *9*, 329–335.
- (39) Glover, K. J.; Whiles, J. A.; Wu, G.; Yu, N.; Deems, R.; Struppe, J. O.; Stark, R. E.; Komives, E. A.; Vold, R. R. *Biophys. J.* **2001**, *81*, 2163–2171.
- (40) Triba, M. N.; Warschawski, D. E.; Devaux, P. F. *Biophys. J.* **2005**, *88*, 1887–1901.
- (41) Kucerka, N.; Liu, Y. F.; Chu, N. J.; Petrache, H. I.; Tristram-Nagle, S.; Nagle, J. F. *Biophys. J.* **2005**, *88*, 2626–2637.
- (42) Lerche, M. H.; Meissner, A.; Poulsen, F. M.; Sørensen, O. W. J. *Magn. Reson.* **1999**, *140*, 259–263.
- (43) Ortega, A.; García de la Torre, J. *J. Chem. Phys.* **2003**, *119*, 9914–9919.
- (44) Cady, S. D.; Goodman, C.; Tatko, C. D.; DeGrado, W. F.; Hong, M. *J. Am. Chem. Soc.* **2007**, *129*, 5719–5729.
- (45) Wüthrich, K.; Wagner, G. *FEBS Lett.* **1975**, *50*, 265–268.
- (46) Lerche, M. H.; Meissner, A.; Poulsen, F. M.; Sørensen, O. W. J. *Magn. Reson.* **1999**, *140*, 259–263.
- (47) Wishart, D. S.; Sykes, B. D.; Richards, F. M. *Biochemistry* **1992**, *31*, 1647–1651.
- (48) Thøgersen, L.; Schiøtt, B.; Vosegaard, T.; Nielsen, N. C.; Tajkhorshid, E. *Biophys. J.* **2008**, *95*, 4337–4347.
- (49) Brünger, A. T.; Adams, P. D.; Clore, G. M.; DeLano, W. L.; Gros, P.; Grossé-Kunstleve, R. W.; Jiang, J. S.; Kuszewski, J.; Nilges, M.; Pannu, N. S.; Read, R. J.; Rice, L. M.; Simonson, T.; Warren, G. L. *Acta Crystallogr.* **1998**, *D 54*, 905–921.
- (50) Petros, A. M.; Mueller, L.; Kopple, K. D. *Biochemistry* **1990**, *29*, 10041–10048.
- (51) Respondek, M.; Madl, T.; Göbl, C.; Golser, R.; Zanger, K. *J. Am. Chem. Soc.* **2007**, *129*, 5228–5234.
- (52) Boheim, G. *J. Membr. Biol.* **1974**, *19*, 277–303.
- (53) You, S.; Peng, S.; Lien, L.; Breed, J.; Sansom, M. S. P.; Woolley, G. A. *Biochemistry* **1996**, *35*, 6225–6232.
- (54) Bechinger, B.; Skladnev, D. A.; Ogrel, A.; Li, X.; Rogozhkin, E. V.; Ovchinnikova, T. V.; O’Neil, J. D. J.; Raap, J. *Biochemistry* **2001**, *40*, 9428–9437.